



Determining N₂O and N₂ fluxes in relation to winter wheat and sugar beet growth and development using the improved ¹⁵N gas flux method on the field scale

Jonas Ecke¹ · Reinhard Well² · Martin Maier³ · Amanda Matson^{2,4} · Klaus Dittert¹ · Pauline Sophie Rummel^{1,5} 

Received: 23 August 2023 / Revised: 23 February 2024 / Accepted: 27 February 2024
© The Author(s) 2024

Abstract

The objectives of this field trial were to collect reliable measurement data on N₂ emissions and N₂O/(N₂O + N₂) ratios in typical German crops in relation to crop development and to provide a dataset to test and improve biogeochemical models. N₂O and N₂ emissions in winter wheat (WW, *Triticum aestivum* L.) and sugar beet (SB, *Beta vulgaris* subsp. *vulgaris*) were measured using the improved ¹⁵N gas flux method with helium–oxygen flushing (80:20) to reduce the atmospheric N₂ background to < 2%. To estimate total N₂O and N₂ production in soil, production-diffusion modelling was applied. Soil samples were taken in regular intervals and analyzed for mineral N (NO₃⁻ and NH₄⁺) and water-extractable Corg content. In addition, we monitored soil moisture, crop development, plant N uptake, N transformation processes in soil, and N translocation to deeper soil layers. Our best estimates for cumulative N₂O + N₂ losses were 860.4 ± 220.9 mg N m⁻² and 553.1 ± 96.3 mg N m⁻² over the experimental period of 189 and 161 days with total N₂O/(N₂O + N₂) ratios of 0.12 and 0.15 for WW and SB, respectively. Growing plants affected all controlling factors of denitrification, and dynamics clearly differed between crop species. Overall, N₂O and N₂ emissions were highest when plant N and water uptake were low, i.e., during early growth stages, ripening, and after harvest. We present the first dataset of a plot-scale field study employing the improved ¹⁵N gas flux method over a growing season showing that drivers for N₂O and N₂O + N₂ fluxes differ between crop species and change throughout the growing season.

Keywords Denitrification · Nitrogen Cycling · N balance · Plant N uptake · Crop development

Introduction

Denitrification is one of the main sources of gaseous N losses to the environment with N₂O and N₂ being its main end products. N₂O is an important greenhouse gas with a global warming potential of 298-times that of CO₂ (Ciais et al. 2014) and emissions of N₂O from agriculture have been monitored for several decades. In contrast, N₂ is inert, and there are very few studies directly measuring N₂ emissions on the field scale. Lack of N₂ fluxes restricts validation and improvement of biogeochemical models (Grosz et al. 2023). Quantifying N₂ losses is crucial to understand denitrification dynamics, N use efficiency of crops, and to develop strategies to mitigate denitrification and N₂O fluxes (Scheer et al. 2020).

Direct quantification of N₂ emissions is quite challenging, particularly due to its high atmospheric background concentrations of 78.1%. The only method that is applicable on the field scale is the ‘¹⁵N gas flux method’ (¹⁵NGF,

✉ Pauline Sophie Rummel
pauline.rummel@bio.au.dk

¹ Department of Crop Science, Plant Nutrition and Crop Physiology, Georg-August-Universität Göttingen, Göttingen, Germany

² Federal Research Institute for Rural Areas, Forestry and Fisheries, Thünen Institute of Climate-Smart Agriculture, Brunswick, Germany

³ Department of Crop Science, Soil Physics, Georg-August-Universität Göttingen, Göttingen, Germany

⁴ Wageningen Environmental Research, Wageningen University & Research, Wageningen, The Netherlands

⁵ Department of Geosciences and Natural Resource Management, Geography, University of Copenhagen, Copenhagen, Denmark

a list of abbreviations can be found in the Supplementary Material). Highly enriched ^{15}N labelled NO_3^- is added to soil allowing monitoring of ^{15}N labelled denitrification products N_2O and N_2 (Siegel et al. 1982). This method has proven to be efficient for monitoring short-term fluxes in pot experiments (Rummel et al. 2021; Kirkby et al. 2023), as well as on the field scale (Buchen et al. 2016; Sgouridis et al. 2016; Friedl et al. 2022; Takeda et al. 2022; Buchen-Tschiskale et al. 2023). Recently, an improved version of the ^{15}N gas flux method ($^{15}\text{NGF}+$) was developed, combining the approaches of the ^{15}N gas flux method and the HeO_2 atmosphere method (Well et al. 2019a; Friedl et al. 2020; Micucci et al. 2023). Prior to accumulation of soil-derived gases, the chambers' headspace is flushed with an artificial HeO_2 atmosphere. This lowers the background concentration of unlabeled atmospheric N_2 and thus improves the limit of detection. It achieves realistic estimates of cumulative denitrification fluxes with sufficient sensitivity to study N_2 and N_2O fluxes on the field scale enabling the study of denitrification responses to control factors. However, measurement of ^{15}N -labelled N_2 and N_2O surface gas fluxes excludes subsoil fluxes and pore space accumulation and thus underestimates total denitrification rates (Sgouridis et al. 2016; Well et al. 2019b). To overcome this, production-diffusion modelling can be applied to calculate total N_2O or N_2 production within the soil column including subsoil fluxes (Well et al. 2019b).

Growing plants exert great influence on denitrification by altering the availability of the main substrates (NO_3^- and C_{org}), as well as moisture and pH value of soils (von Rheinbaben and Trolldenier 1984; Malique et al. 2019; Rummel et al. 2021). Water uptake and transpiration by plants decrease soil moisture, thus decreasing the anaerobic soil volume and denitrification (Firestone and Davidson 1989; Buchen et al. 2016; Rummel et al. 2021). In contrast, root respiration and increased microbial activity caused by rhizodeposition can increase O_2 consumption in the rhizosphere and therefore denitrification (Klemmedtsson et al. 1987; Groffman et al. 1988; Hamonts et al. 2013; Senbayram et al. 2020). The amount of C_{org} transferred into the soil depends on plant species, age, and development (Kuzuyakov and Domanski 2000). Pot-scale studies suggest that plant growth may stimulate denitrification during early growth phases (Senbayram et al. 2020) and senescence (Klemmedtsson et al. 1987), while N and water uptake of plants are limiting factors for denitrification during vegetative growth phases (Haider et al. 1985; Rummel et al. 2021). Plant and root development strongly differ between crop species, especially when comparing winter with summer crops or cereals with root and tuber crops. Accordingly, the time course of N_2O emissions differs between crop species (Jeuffroy et al. 2013; Ruser et al. 2017). The few available field studies indicate that N_2 fluxes do not follow the same patterns as

N_2O fluxes leading to fluctuations in denitrification product ratios throughout the season (Buchen et al. 2016; Friedl et al. 2023; Takeda et al. 2023).

This study aimed (i) to test the novel improved ^{15}N gas flux method with production-diffusion modelling on the field scale, (ii) to quantify N_2O and N_2 fluxes and production rates on the field scale and the influence of the growth of two plant species that differ in their spatial and temporal biomass development. (iii) Further, we aimed at generating a full dataset to be used for optimization and validation of N_2 fluxes in modelling as proposed by Grosz et al. (2021). We hypothesized, that growth and development patterns of different plant species control all drivers of denitrification (O_2 , NO_3^- , and C_{org} availability, temperature) and therefore N_2O , and N_2 losses and $\text{N}_2\text{O}/(\text{N}_2\text{O} + \text{N}_2)$ ratios. In detail, we expect that (1) plant N uptake governs NO_3^- availability for denitrification leading to higher N_2O and N_2 emissions when plant N uptake is low. (2) Increasing C availability increases denitrification derived N losses and decreases the $\text{N}_2\text{O}/(\text{N}_2\text{O} + \text{N}_2)$ ratio. And (3) denitrification-promoting effects of C_{org} supply to soil by rhizodeposition are inferior to denitrification-lowering effects caused by plant uptake of NO_3^- and water.

Methods

Study site and crop management

The experiment was conducted on the experimental farm "Reinshof" of the Georg-August University Göttingen, Germany (51.499°N, 9.931°E, 157 m a.s.l.) during 2021. The mean annual temperature of the area is 9.3 °C and the mean annual precipitation is 628 mm (30-year mean, 1992 to 2021, (DWD 2021)). The precrop grown on the field site in the year before the experiment was winter barley (*Hordeum vulgare* L.). The soil at the site is classified as luvisol developed from loess. For the experiment, the field was split in two sections to grow two different crops winter wheat (**WW**, *Triticum aestivum* L.) and Sugar beet (**SB**, *Beta vulgaris* L.). Although the two sections were only ~ 10 m apart, soil texture and pH were slightly different. The more northern WW section was classified as silt loam (19% sand, 60% silt, 21% clay) with a pH (CaCl_2) of 7, while the more southern SB section was classified as silty clay loam (SB: 23% sand, 49% silt, 29% clay) with a pH (CaCl_2) of 7.5.

Winter wheat (cv. RGT Reform, 300 seeds per m^2) was sown in October 2020 after incorporation of barley stubbles. After wheat was harvested in August 2021, stubbles were mulched, and phacelia (*Phacelia tanacetifolia* Benth.) was sown as cover crop in September 2021. On the other section, a catch crop mixture of phacelia (*Phacelia tanacetifolia* Benth.), oil flax (*Linum usitatissimum* L.), and niger

seed (*Guizotia abyssinica* (L.F.) Cass.) was established in August 2020 and mulched in March 2021. Sugar beet was sown in late March 2021 (cv. Thaddea KWS, row distance 45 cm, seed distance 21 cm). Due to the low germination rates caused by cold temperatures in April, manual re-sowing was done in the beginning of May. Sugar beets were harvested at the end of September, and shredded leaves were incorporated into the soil. Pest management followed regional standards and best management practice in both crops (Supplementary Table S1). Winter wheat did not receive any other nutrients during the experimental period, sugar beet were fertilized with 166 kg K ha⁻¹, 73 kg P ha⁻¹, 61.6 kg Mg ha⁻¹, and 26 kg S ha⁻¹.

Experimental design and ¹⁵N application

For each crop, 6 macroplots (WW: 3 m × 8 m, SB: 3 m × 11 m) were defined. Within each macroplot, a mesoplot (1.4 m × 1.4 m) and a microplot (∅ 30 cm) were established (Supplementary Fig. S1). In the mesoplots, we applied low ¹⁵N enrichment labeling (~5 at%) to determine fertilizer-derived plant N uptake and to trace translocation of fertilizer N in soil. The microplots were fertilized with high ¹⁵N enrichment (~60 at%) and used for gas sampling. For WW, microplots were chosen where uniformly growing plants were present, for SB one representative plant was identified. Meso- and microplots remained at the same spot throughout the growing seasons. Both crops were fertilized according to their N demand and yield potential, typical for these crops in the region. WW was fertilized with 21 g N m⁻² (equivalent to 210 kg N ha⁻¹) split in two fertilizer doses of 14 g N m⁻² on April 8th and 7 g N m⁻² on June 11th. After wheat harvest, phacelia was fertilized with 3 g N m⁻² on September 6th. SB was fertilized with 10 g N m⁻² (equivalent to 100 kg N ha⁻¹) split in two fertilizer doses of 5 g N m⁻² each on May 20th and July 6th. Application technique and formulation of the fertilizer differed between macro-, meso-, and microplot.

Microplots were fertilized with a ¹⁵N enriched tracer solution made of ¹⁵N-labeled Ca(NO₃)₂ (~60 at% ¹⁵N₂, Campro Scientific GmbH, Berlin, Germany) dissolved in H₂O_{dest}. To ensure homogenous label distribution in the upper 20 cm of the microplots, we aimed to completely exchange soil water inside the upper 20 cm of the microplots with the tracer solution. Based on the findings of pre-experiments with similar soil properties to the field site, the 1.6-fold of the present soil water solution was applied to replace ~80% of soil water with the tracer solution. The necessary amount of water was estimated based on soil water content prior to each fertilization event. The tracer solution was applied as evenly as possible with drip irrigation in intervals (15 min application, 45 min pause) using a sprinkling head with 163 sprinkling capillaries (EcoTech, Bonn, Germany) connected

to a peristaltic pump (ISM444B, Ismatec, Wertheim, Germany) to ensure infiltration into soil. Thus, for all fertilization events, two consecutive days with ~8 h of irrigation were needed.

Mesoplots were fertilized with a ¹⁵N enriched tracer solution made of ¹⁵N-labeled Ca(NO₃)₂ (~5 at% ¹⁵N₂, Campro Scientific GmbH, Berlin, Germany) dissolved in H₂O_{dest}. To distribute the tracer solution evenly, the mesoplot was divided into 100 small squares and aliquots of the fertilizer solution were distributed with a dispenser. Afterwards, mesoplots were carefully irrigated to facilitate infiltration and distribution of the fertilizer into the soil and to increase soil water content similarly to microplots. In the macroplots, N was added as conventional solid calcium ammonium nitrate and macroplots were irrigated in intervals using a garden sprinkler.

Plant and soil sampling and analyses

An overview of plant and soil samples taken and analyzed during the experiment is given in Table 1. Detailed description of the procedures can be found in the Supplementary Material.

Determination of N₂O and N₂ fluxes

Chamber design, gas sampling setup, and static chamber method

Prior to the experiment, PVC cylinders (30 cm inner diameter, 32 cm length, 8 mm wall thickness) were inserted to a depth of 30 cm into the soil in each microplot. A seventh cylinder was installed next to the macroplots for each crop. These were fertilized like the other microplots and used for soil sampling before/after fertilization. After installing the cylinders, a ring of 6 cm height with a slanted edge, fitting precisely into the chamber, was glued on top of the cylinder. Chambers were made from PVC and measured 30 cm in diameter with a height of 35 cm. The chamber was equipped with four ports with Luer-lock stopcocks to enable flushing of the headspace with artificial atmosphere as well as a connection for gas sampling. As the plants grew, the height of the chambers was adjusted to 60 cm (SB) or 90 cm (WW). To prevent diffusion of N₂ from the subsoil into the N₂-depleted headspace, six stainless steel needles were inserted 22 cm into the soil and flushed with artificial atmosphere during chamber closing. The needles were sealed at the lower end and had a side hole at 21 cm depth to allow gas flow into the soil. Needles were removed for tillage after WW and SB harvest and inserted again to depths of 22 cm and 14 cm (incorporation depth of SB leaves), respectively.

Gas fluxes were measured in WW plots from Mid-April to end of October (total experimental period of 197 days) and

Table 1 Overview of plant, soil, and meteorological data collected during the field trial. A detailed description of the measurements can be found in the Supplementary Material

Parameter	how	where	when/how often	references
Above ground plant biomass	Canopeo App	Mesoplot	Weekly until canopy closure	Patrignani and Ochsner 2015
Sugar beet biomass (below-ground)	Harvest, weighing, drying	Macroplot or mesoplot	Monthly	
N content and ^{15}N content of plant biomass	IRMS analysis of dried plant material	Mesoplot	Monthly	
Soil mineral N (NO_3^- , NH_4^+)	2 M KCl extraction (1:4 w/v)	Macroplot 0–30 cm depth Mesoplot 0–30, 30–60, 60–90 cm depth Microplots 0–30, 30–60, 60–90 cm depth	Weekly 4-weekly End of experiment	
^{15}N enrichment in NO_3^- , NH_4^+	IRMS analysis of soil extracts (2 M KCl)	Mesoplot 0–30, 30–60, 60–90 cm depth	4-weekly	Eschenbach et al. 2017, 2018; Dyckmans et al. 2021
Water-extractable organic C (WEOC)	Extraction with ultrapure water (1:5 w/v)	Macroplot 0–30 cm depth Mesoplot 0–30, 30–60, 60–90 cm depth	weekly 4-weekly	
Soil moisture and temperature	FDR sensors (ECH2O 5TM, Decagon Devices, Pullman, USA)	5 replicates in each crop, 5–10 cm depth	30-min intervals	
Air temperature	ATMOS 14 temperature sensor (Meter Group, Pullman, USA)	~ 100 m next to field site	1-h intervals; end of April—Mid-October	
Daily precipitation	ECRN-100 Rain Gauge (Meter Group, Pullman, USA)			
Air temperature, daily precipitation	Weather station of Germany's Meteorological Service (ID: 1691)	~ 1.3 km from field site	1-h intervals; April and end of October	

in SB plots from Mid-May to end of October (154 days). Gas samples from microplots were collected in intervals of one or two weeks. To determine N_2O fluxes, the closed-chamber method (Hutchinson and Mosier 1981) was used. Sampling was always performed in the morning hours between 8 and 10 am. Chambers were closed, sealed, and headspace atmosphere of the chamber was sampled in intervals of 0, 20, 40, and 60 min. For larger chambers, sampling intervals were extended to 80 min (SB) or 80 and 100 min (WW).

In addition, we applied a novel improved version of the ^{15}N gas flux method ($^{15}\text{NGF}+$) (Well et al. 2019a) to directly determine N_2O and N_2 emissions in the field. For both gas sampling techniques, the same chambers and collars were used. When both methods were applied on the same day, the closed-chamber samples were always taken prior to the $^{15}\text{NGF}+$ to prevent disturbances by headspace and soil flushing and enable comparisons between the N_2O measurements of both methods. All gas samples were taken by connecting a handheld electric air pump to the chamber and pumping the headspace atmosphere through a glass Exetainer (12 ml, Labco, High Wycombe, UK) and back into the chamber. Exetainers were flushed for one

minute to exchange the vial volume > 40 times, then increasing the pressure in the exetainer to ~2.5 bar.

^{15}N gas flux method

For the ^{15}N gas flux method ($^{15}\text{NGF}+$), a gas mixture consisting of 80% He and 20% O_2 (Air products, Hattingen, Germany; purity of N4.6 for He and N2.5 for O_2) was used to replace the headspace atmosphere before sampling. Gases were mixed by two digital flow controllers (MC-5SLPM-D for O_2 , MC-20SLPM-D for He, Alicat Scientific, Tucson, Arizona, USA). Two chambers were flushed with the gas mixture at the same time and two gas flow meters (Minimaster MMA-25 and Minimaster MMA-20, Dwyer Instruments Inc, Michigan City, Indiana, USA) installed between the chamber and the incoming gas matrix ensured equal gas flow into both chambers.

The sampling routine for $^{15}\text{NGF}+$ consisted of three phases: 1) high-flow headspace flushing, 2) low-flow headspace flushing, and 3) headspace accumulation with subsoil flushing. In phase one, the headspace atmosphere was exchanged by flushing the chamber for 15 min with a flow rate of 12 L min^{-1}

with open outflow at a second port. This phase of fast flushing aimed to reduce the atmospheric N_2 background in the chamber and in the pore volume of the labelled soil to below 2%. Depending on soil moisture and air conductivity a variable fraction of the inflow leaves the chamber via the exhaust while the remainder is flushing the soil vertically (Well et al. 2019a). For the next three minutes, the outflow port was closed, and the flushing rate reduced to 3 L min^{-1} . The reason for adding this phase is to ensure vertical flushing of the soil in case of high moisture and thus low gas conductivity since the gas is forced into the soil when the exhaust port of the chamber is closed. During the accumulation phase, the steel needles were flushed with the gas mixture with a flow rate of 0.3 L min^{-1} . This subsoil flushing aimed to inhibit diffusion of N_2 from the subsoil into the chamber. During the accumulation phase, headspace samples were taken in intervals of 0, 20, 40, and 60 min. For larger chambers, sampling intervals were extended to 80 min (SB) or 80 and 100 min (WW). At the end of the closure period, triplicate headspace samples were taken as described above. One of the samples was analyzed by gas chromatography, the other by isotope ratio mass spectrometry (IRMS), and the third used as backup for IRMS.

As only two chambers could be flushed at once, chambers were always flushed and sampled in pairs (1 and 2, 3 and 4, 5 and 6) with the sampling order changing every week. When the height of chambers was increased, flushing rates and times were adjusted to 20 min high-flow flushing with 15 L min^{-1} and 5 min low-flow flushing with 3.75 L min^{-1} . Needle flushing rates were not altered.

Gas analysis and N_2O flux calculations

Samples from both methods and all sampling intervals were analyzed for N_2O and CO_2 concentrations by gas chromatography (GC-2014, Shimadzu, Kyoto, Japan) equipped with a thermal conductivity detector (TCD) measuring CO_2 and an electron capture detector (ECD) measuring N_2O . N_2O and CO_2 fluxes were calculated using the R software (R Core Team 2022) including the package *gasfluxes* v.0.4–4 (Fuß 2020). Briefly, molar gas concentrations were transformed into mass concentrations according to the ideal gas law. The most appropriate flux calculation model was selected based on the Akaike information criterion (AIC) and the kappa value, choosing between a linear model, a nonlinear HMR model, and a robust linear regression model. Resulting gradients were multiplied with the chamber volume divided by chamber area to derive gas flux estimates. To estimate the reliability of the diffusive gas accumulation in the chambers, CO_2 concentration gradients were used. Calculated fluxes were discarded if the Pearson coefficient of the CO_2 flux was smaller than +0.85. N_2O fluxes with standard errors above $100 \mu\text{g N m}^{-2} \text{ h}^{-1}$ were also discarded (Ruser et al.

2017). About 4.5% of all measured fluxes did not meet these criteria. N_2O fluxes calculated from the static chamber method will be referred to as N_2O and N_2O fluxes calculated from HeO_2 flushed chambers are referred to as N_2O_{heox} . Cumulative N_2O emissions were calculated by linear interpolation of fluxes.

Isotopic analysis and calculation of N_2 and N_2O

To determine N_2O , N_2 , and $N_2O + N_2$ fluxes derived from the ^{15}N -labeled N pool, gas samples collected at the 60 min sampling interval (80 or 100 min for larger chambers) were analyzed for m/z 28 ($^{14}\text{N}^{14}\text{N}$), 29 ($^{14}\text{N}^{15}\text{N}$) and 30 ($^{15}\text{N}^{15}\text{N}$) of N_2 using a modified GasBench II preparation system coupled to an isotope ratio mass spectrometer (MAT 253, Thermo Fisher Scientific, Bremen, Germany) according to Lewicka-Szczebak et al. (2013). This system allows a simultaneous determination of mass ratios ^{29}R (29/28) and ^{30}R (30/28) of $N_2 + N_2O$, N_2 and N_2O , all measured as N_2 gas after N_2O reduction in a Cu oven. Reproducibility of ^{29}R and ^{30}R (standard deviation of 4 replicate standard samples) was typically $< 1 \times 10^{-6}$ and 5×10^{-6} , respectively. N_2 concentration in the samples analyzed on MAT 253 IRMS ranged between 0.35 and 27.99% with a mean of $1.33 \pm 2.55\%$ N_2 . The detection limit for N_2O was between 0.2 and 1 ppm depending on the ^{15}N enrichment of the sample. For dates with high N_2O concentrations but undetectable N_2O peak by analysis with MAT 253 IRMS, additional samples were analyzed for isotopocule values of N_2O using a Delta V isotope ratio mass spectrometer (Thermo Scientific, Bremen, Germany) coupled to an automatic preparation system with a Precon + Trace GC Isolink (Thermo Scientific, Bremen, Germany), where N_2O was pre-concentrated, separated and purified, as described previously (Lewicka-Szczebak et al. 2014). In this setup, m/z 44, 45, and 46 of the intact N_2O^+ ions were determined, and ^{29}R and ^{30}R were derived from them (Bergsma et al. 2001; Deppe et al. 2017). Data were normalized against background values of a breathing air laboratory standard. Analysis of ^{15}N -labelled standard gases confirmed detectable ap_{N_2O} and Fp_{N_2O} values for N_2O concentrations > 0.1 ppm.

The fraction originating from the ^{15}N -labeled pool with respect to total N in the gas sample (F_p) was calculated after Mulvaney (1984) using data from MAT 253 IRMS for all sampling dates:

$$F_p = ({}^{29}\text{R}_{\text{sa}} - {}^{29}\text{R}_{\text{bgd}}) / (2 \cdot ap^* (1 - ap)) \quad (1)$$

where lower case sa and bgd denote sample and background, respectively and ap is the ^{15}N enrichment of the ^{15}N -labeled N pool undergoing denitrification. Variables of Eq. 1 were calibrated and normalized as described by Buchen-Tschiskale et al. (2023). Briefly, gas samples from

the unlabeled microplots were used as background to determine $^{29}\text{R}_{\text{bgd}}$ and sample measurements were corrected with standard gases. If available, ap-values from Delta V measurements were used for calculations, otherwise ap-values from MAT 253 IRMS measurements were used. For samples without measured ap-values, the mean value from the other replicates from the same sampling date was used. To obtain ^{15}N -pool-derived gas concentrations (in ppm), Fp values were multiplied with respective total sample N concentration to obtain concentrations of ^{15}N -pool-derived N species in the sample gas (fp values, i.e. fp_{N₂O}, fp_{N₂}, fp_{N₂O + N₂}). Then, fluxes derived from the ^{15}N -labeled NO₃⁻ pool undergoing denitrification were calculated from fp values assuming linear increase over the accumulation time and will be referred to as ^{15}N -pool derived fluxes.

For dates with Delta V measurements, Fp_{N₂O} and fp_{N₂O} was calculated from the non-equilibrium distribution of N₂O isotopocules according to Bergsma et al. (2001) and Spott et al. (2006).

Denitrification product ratio was calculated based on Eq. 2.

$$\text{Denitrification product ratio} = \text{fp}_{\text{N}_2\text{O}} / \text{fp}_{\text{N}_2\text{O} + \text{N}_2} \quad (2)$$

For certain samples, significant fp_{N₂O + N₂} values were detected while fp_{N₂} and fp_{N₂O} were below detection because δ¹⁵N values of N₂O + N₂ were higher than of N₂. Therefore, the number of evaluable datapoints for ^{15}N -pool-derived N₂O was more limited. To allow evaluation of samples with and without detectable fp_{N₂} and fp_{N₂O}, we calculated an auxiliary ratio using total N₂O from GC measurements (Eq. 3):

$$\text{Total N}_2\text{O ratio} = \text{N}_2\text{O}_{\text{heox}} / \text{fp}_{\text{N}_2\text{O} + \text{N}_2} \quad (3)$$

As product ratios have been shown to be unaffected by the flushing method (Well et al. 2019a), it is possible to calculate N₂O + N₂ losses from N₂O fluxes and product ratios:

$$\text{N}_2\text{O} + \text{N}_2_{\text{est}} = \text{N}_2\text{O} / \text{total N}_2\text{O ratio} \quad (4)$$

The fraction of N₂O + N₂ derived from fertilizer was calculated by dividing ap_{N₂O} by the ^{15}N enrichment of applied fertilizer (60 at%). Then, fertilizer-derived N₂O + N₂_{fert}

fluxes were calculated by multiplying N₂O + N₂_{est} with this fraction. Cumulative emissions were calculated by linear interpolation of fluxes.

Production-diffusion modelling

To determine total production rates of ^{15}N -pool-derived N₂ and N₂O from chamber fluxes, storage in pore space of the labelled soil and downward diffusion must be taken into account. Previously, production-diffusion modeling using numerical finite element modelling (FEM) with the program COMSOL Multiphysics (Version 5.2, COMSOL Inc., Burlington, Massachusetts, US) was conducted to realize this for the ^{15}N gas flux method under ambient atmosphere (Well et al. 2019b). Here, we adapted this FEM model to the improved ^{15}N gas flux method (Well et al. 2019a) by using diffusivity for Helium–Oxygen mixture (Katz et al. 2011) and adapting the chamber geometries. Our modelling assumed homogenous distribution of diffusivity, labeled NO₃⁻, and of N₂ and N₂O production because we only had data on average values of moisture and bulk density over all replicates and no data to estimate depth-dependence of denitrification activity. Moreover, we assumed that continuous needle flushing at 20 cm depth would enhance downward diffusion of ^{15}N -pool-derived N₂ and N₂O as the downward convection of the injected gas mixture would keep their concentration close to zero. In the FEM model, this was taken into account by defining artificially high gas diffusions coefficients (100 times of diffusivity in free air) in the surrounding soil which resulted in a lower boundary condition of close to zero concentration at 20 cm depth. Production thus results from the sum of chamber flux plus the subsurface flux, i.e. the sum of storage and subsoil diffusion fluxes. The FEM model was run for the different chamber geometries and all potentially relevant parameters to generate a dataset which eventually allowed deriving a correction factor. Correction factors were calculated for each individual date by using actual chamber geometry and air-filled pore space as derived from water content and bulk density. We then calculated total production rates (N₂O + N₂_{prod}, N₂_{prod}, N₂O_{prod}, mg N m⁻² d⁻¹) for N₂O + N₂, N₂, and N₂O fluxes according to Eq. 5:

$$\text{Production rate} = \text{flux}_{\text{measured}} * (1 - (\text{chamber}_{\text{flux}_t} * a + \text{AFPS}_t * b + \text{Intercept})) \quad (5)$$

where *chamber_{flux_t}* is the measured chamber flux at each measured time point (N₂O, N₂, or N₂O + N₂ in mol N m⁻² s⁻¹), and *AFPS_t* is the air-filled pore space at this respective time point (in m³/m³). The fit parameter a, b, and intercept were derived from the dataset generated by

the parameter sweeps of the FEM Model and were slightly different for each chamber geometry. Total cumulative N₂O_{prod} or N₂O + N₂_{prod} production was calculated by linear interpolation of production rates.

Statistics

All statistical analyses were performed using the statistical software R version 4.0.3 (R Core Team 2022). p -values < 0.05 were considered statistically significant. Means and standard errors were calculated over all ^{15}N labelled replicates ($n = 5$). Differences in cumulative N_2O , $\text{N}_2\text{O} + \text{N}_2$, $\text{N}_2\text{O} + \text{N}_2_{\text{prod}}$, $\text{N}_2\text{O} + \text{N}_2_{\text{est}}$, and $\text{N}_2\text{O} + \text{N}_2_{\text{fert}}$ between crops were compared using a t -test or a Mann–Whitney U test when data were not normally distributed.

To test the combined effect of soil environmental variables (soil temperature, soil moisture, N_{min} , WEOC) on N_2O and $\text{N}_2\text{O} + \text{N}_2_{\text{est}}$ fluxes, generalized additive models (GAM) were applied as implemented in the R package mgcv version 1.8–41 (Wood and Augustin 2002; Wood 2011). N_2O and $\text{N}_2\text{O} + \text{N}_2_{\text{est}}$ fluxes were log-transformed, which is a common prerequisite for analyzing N_2O data because of their skewed distribution (Folorunso and Rolston 1984). As total N_2O ratios are distributed between 0 and 1, we applied beta regression models using the R package betareg version 3.0–55 (Cribari-Neto and Zeileis 2010). Best models were selected using AICc (Akaike's information criterion). We excluded the SB post-harvest period

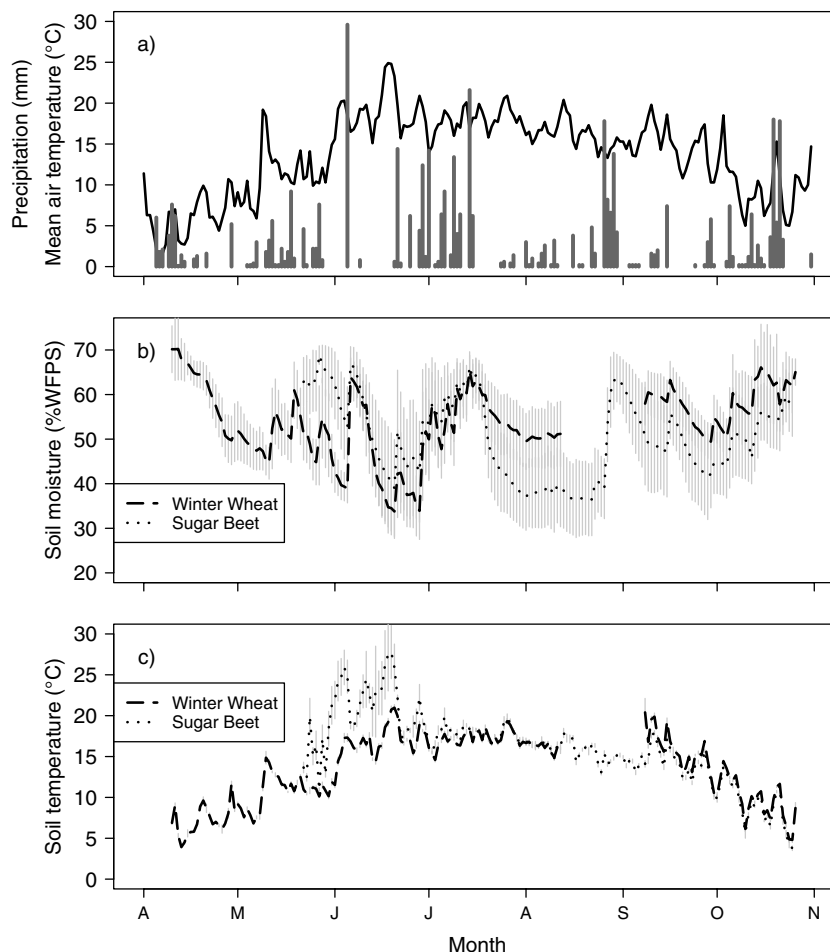
from the dataset for GAM. N_2O and N_2 production after litter addition is largely driven by local oxygen shortage due to increased microbial respiration (Parkin 1987; Chen et al. 2013; Kravchenko et al. 2018) and it was considered unlikely that the SB post-harvest period could be explained by the same relationships. However, data from the SB post-harvest period were not sufficient for statistical analysis.

Results

Meteorological data, soil moisture and temperature

At the Reinshof field site, the annual precipitation during the meteorological year of 2021 (01.11.2020 to 30.10.2021) was 581.2 mm. During the period of gas measurements, daily mean air temperatures ranged from 4.4 °C to 24.9 °C (Fig. 1). Recorded soil temperatures at five cm depth ranged from 4.84 °C to 21.78 °C in WW and from 4 °C to 28.54 °C in SB. WFPS ranged between 33.91% and 70.31% in WW and between 35.38% and 66.32% in SB (Fig. 1).

Fig. 1 Time course of (a) mean daily air temperature and precipitation, (b) soil moisture as water-filled pore space (%WFPS), and (c) and daily soil temperature in 5 cm depth at 10 am (b + c: mean \pm standard deviation for $n = 5$)



Soil moisture and temperature were affected by plant growth and development. In the first half of the measurement period (until mid-July) soil moisture was lower in WW compared to SB (Fig. 1). From mid-July until the end of the experiment, soil moisture was higher in SB. Soil temperatures were higher in SB until the end of June.

Crop development

The development of plant biomass of WW and SB is shown in Fig. 2 a + b. Canopy cover and above ground biomass of WW increased almost linearly from April until canopy closure at the end of May. On the day of WW harvest (August 9th), total aboveground plant biomass was 2418.3 ± 207.0 g DM m^{-2} in the mesoplots. Grain yield on the mesoplots was 657.6 ± 93.0 g DM m^{-2} (Supplementary Table S2). Plant growth in the macroplots was uneven and the mesoplots had been established in the more homogeneous parts of the macroplots. In the microplots, total aboveground plant biomass and grain yield were lower with 1488.8 ± 187.2 g DM m^{-2} and 453.4 ± 204.0 g DM m^{-2} respectively. Likely

reasons are the confinement in the microplots which restricted available soil area. Further, gas sampling with chambers may have disturbed plant growth leading to lower yields. In contrast, phacelia dry mass at the end of the experiment was higher in microplots, likely due to differences in plant density from manual sowing.

Cold temperatures in spring led to slow and irregular SB germination and affected crop development of SB. Six weeks after sowing, plants were only in 3- or 4-leaf stadium (BBCH-scale 11 and 12, Lancashire et al. 1991) with ~3% canopy cover. On the first sampling date (May 21st), SB biomass was 3.2 ± 1.9 g DM m^{-2} . Leaf biomass increased slowly during the first months. With increasing temperatures in June, SB leaf growth increased strongly until end of August. SB beet biomass stayed low on the first two sampling dates, then increased strongly until end of August. At SB harvest, total SB biomass was 2573.2 ± 155.0 g DM m^{-2} (547.2 ± 41.5 g DM m^{-2} leaves, 2026.0 ± 118.2 g DM m^{-2} beet). Average beet dry weight at harvest was slightly higher in microplots (219.2 ± 38.3 g DM) than in mesoplots (187.9 ± 51.0 g DM).

Fig. 2 Time course of (a + b) biomass development of winter wheat and sugar beet, (c + d) soil water-extractable organic C (WEOC) in the upper 0–30 cm soil layer, and (e + f) soil NO_3^- content in 0–30 cm soil layer. Arrows indicate dates of N fertilization (F) and harvest (H) (mean \pm standard deviation for $n=5$)

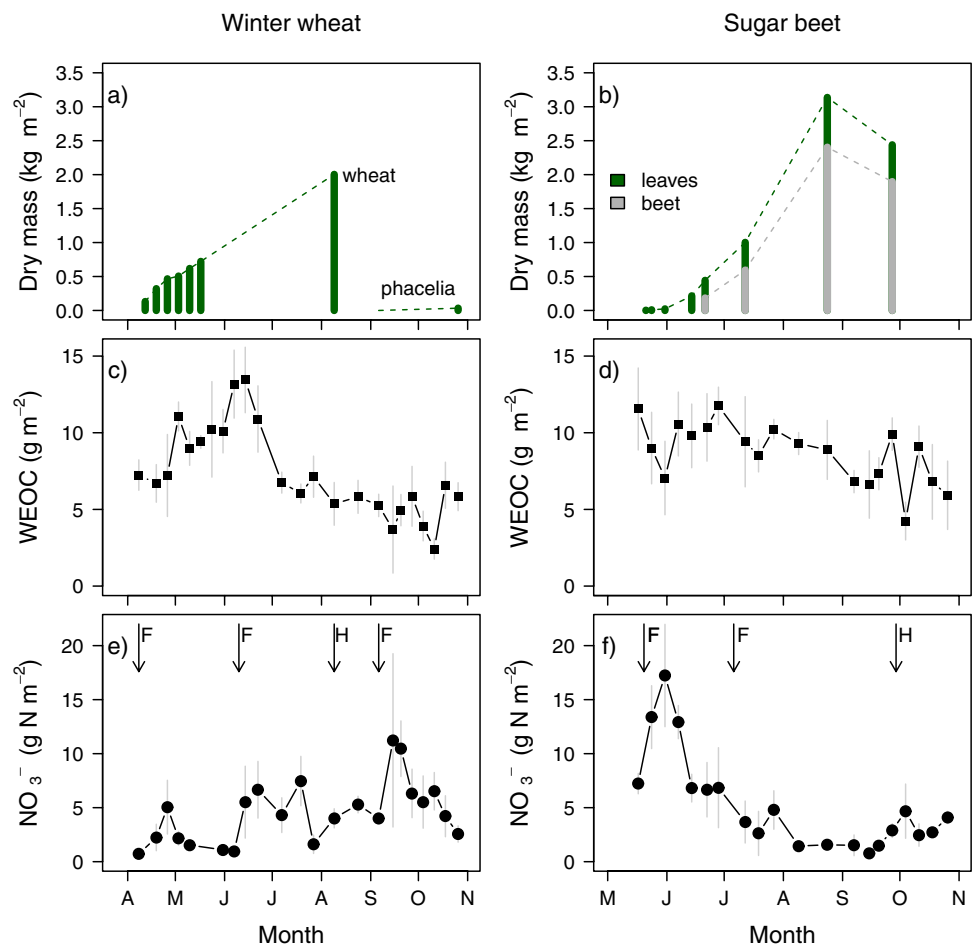
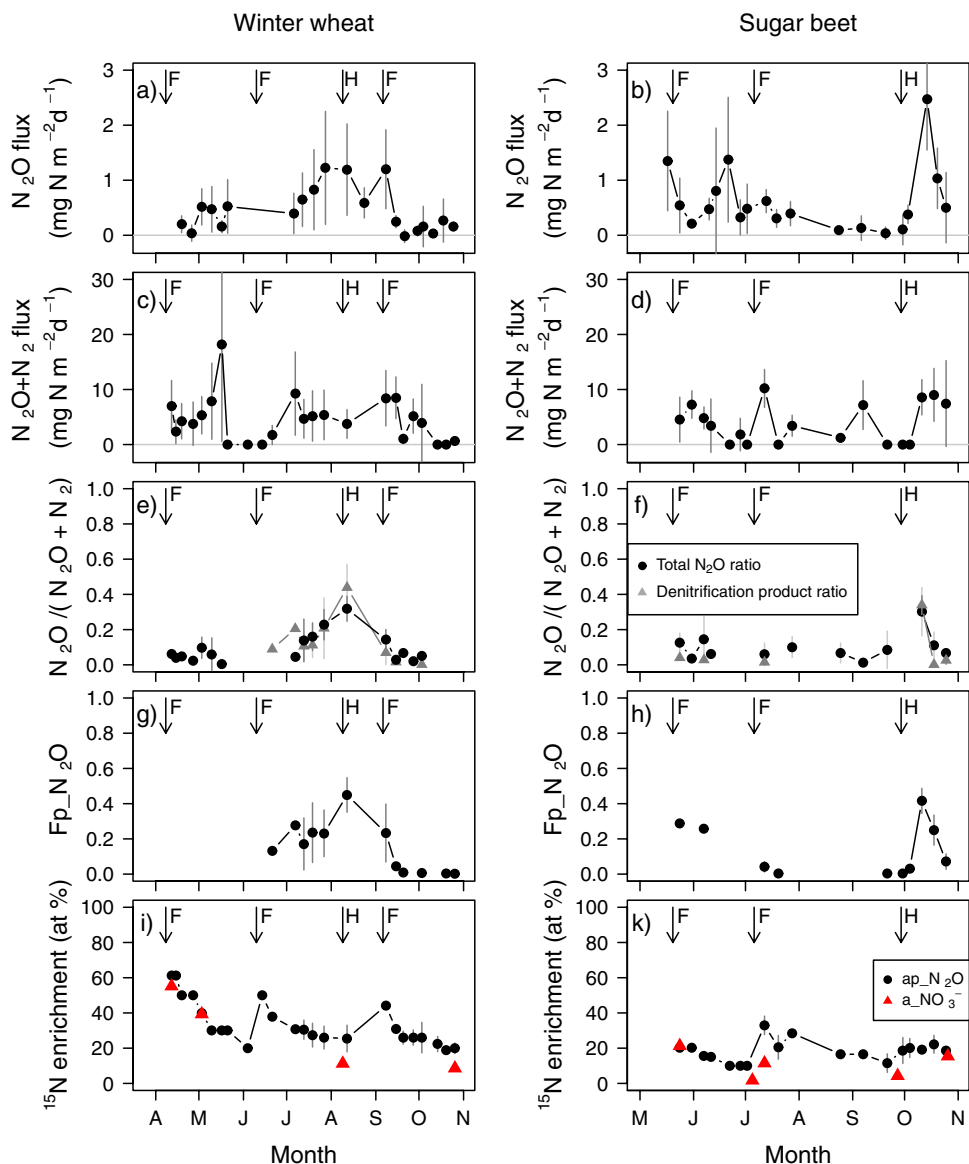


Fig. 3 a + b: N_2O fluxes from winter wheat and sugar beet plots, c + d: best-estimate $N_2O + N_2$ fluxes, e + f: denitrification product ratio (grey) and total N_2O ratio (black). g + h: Fraction of ^{15}N -pool-derived N_2O (Fp_N_2O). i + k: ^{15}N enrichment of the ^{15}N -labelled NO_3^- pool undergoing denitrification ap_N_2O (black) and the total soil NO_3^- pool $a_NO_3^-$ (red triangles) in the microplots in 0–20 cm depth. Vertical arrows show dates of fertilization (F) and harvest (H). Mean \pm standard deviation for $n=5$



Soil water-extractable organic C, mineral nitrogen, and ^{15}N enrichment of N-pools

The dynamics of the WEOC content in WW and SB are shown in Fig. 2 c + d. In WW, the soil WEOC content in the 0–30 cm soil layer increased until Mid-June. Then, it decreased to values similar to spring conditions and only slightly changed after that. Initial soil WEOC content in SB was higher than in WW in the beginning of the experiment. It decreased throughout the growing season, reaching its lowest values after harvest.

The dynamics of the soil NO_3^- content and its ^{15}N enrichment in are shown in Fig. 2 e + f (0–30 cm depth) and Supplementary Figure S3 (0–90 cm depth). In the beginning of the experiment, soil mineral N content was highest in the 60–90 cm soil layer in WW. NO_3^- content and its ^{15}N

enrichment in the upper 0–30 cm topsoil layer increased with each fertilization event. Translocation of labeled NO_3^- to soil layers > 30 cm became only relevant during WW ripening and after harvest. In SB, the soil mineral N content in the upper 0–30 cm topsoil layer was 7.53 g N m^{-2} prior to the first fertilization event. The first N fertilization led to a strong increase in mineral N, while the second fertilization did not cause any increase of the soil mineral N content. After SB harvest and SB leaf incorporation, mineral N values slightly increased. The mineral N content of the 30–60 cm soil layer and the 60–90 cm soil layer showed similar dynamics as the 0–30 cm layer. The ^{15}N enrichment of the NO_3^- pool in the SB mesoplots followed a similar pattern as the total NO_3^- content. Soil NH_4^+ content of both crops was mostly $< 0.5 \text{ g N m}^{-2}$ with low ^{15}N enrichment ($< 0.5\%$ APE, Supplementary Figure S4).

N₂O and N₂O + N₂ fluxes, and ¹⁵N enrichment

Total N₂O fluxes (mg N m⁻² d⁻¹) from WW and SB micropots are shown in Fig. 3 a + b. Directly after the first fertilization in WW, N₂O fluxes remained very low, but slightly increased in May. From the beginning of July, N₂O fluxes increased almost linearly reaching highest values shortly before WW harvest (1.225 mg N m⁻² d⁻¹ on July 28th). Right after harvest, N₂O fluxes remained high, slightly decreased in September and increased again right after sowing and fertilization of phacelia (1.199 mg N m⁻² d⁻¹ on September 8th). In SB, N₂O fluxes were very high before the first fertilization (1.349 mg N m⁻² d⁻¹ on May 17th), then decreased until the beginning of June, and then increased again reaching a peak on June 21st (1.373 mg N m⁻² d⁻¹). After the second fertilization, N₂O fluxes remained low throughout the summer months. After SB harvest and leaf incorporation into the soil, N₂O fluxes increased strongly reaching highest N₂O fluxes in the overall experiment (2.471 mg N m⁻² d⁻¹ on October 14th).

N₂O fluxes derived from the ¹⁵N-labelled NO₃⁻ pool undergoing denitrification could only be determined from mid-June to the beginning of October in WW (Supplementary Figure S5). During this period, they followed a very similar pattern as total N₂O fluxes. In SB, only 6 sampling days were evaluable for N₂O fluxes from the ¹⁵N-labelled NO₃⁻ pool undergoing denitrification which fit the pattern of total N₂O fluxes.

Our best estimates for N₂O + N₂ losses (N₂O + N₂_est) are shown in Fig. 3 c + d. Measured N₂O + N₂ and modelled N₂O + N₂_prod followed similar patterns (Supplementary Figure S5). After the first fertilization in WW, N₂O + N₂_est increased reaching highest fluxes of 18.17 mg N m⁻² d⁻¹ on May 17th followed by three weeks with fluxes below the detection limit. From Mid-July until Mid-September, N₂O + N₂_est ranged between 3.75 and 9.25 mg N m⁻² d⁻¹ and then decreased until the end of the experiment. N₂ fluxes were only evaluable from Mid-June until the beginning of October (Supplementary Figure S5) and followed a similar pattern as N₂O + N₂ fluxes. In SB, N₂O + N₂_est ranged between 1.25 and 10.19 mg N m⁻² d⁻¹ with increases after both fertilization events and SB harvest. N₂ fluxes from SB were only evaluable on 6 days during the experiment with high fluxes in June and low fluxes in October.

The total N₂O ratio showed a similar pattern as the denitrification product ratio (Fig. 3 e + f). In the beginning of the WW growing period, total N₂O ratio was lower than 0.1 except for a short increase in the beginning of May. From mid-June, total N₂O ratio and denitrification product ratio increased to 0.32 and 0.45, respectively, and then decreased until the end of the experiment. Total N₂O ratio in SB was mostly stable with values around 0.1. After SB harvest and incorporation of leaves, the total N₂O ratio and

denitrification product ratio increased to ~0.3 for one sampling day.

The ¹⁵N enrichment of the ¹⁵N-labeled NO₃⁻ pool producing N₂O (ap_N₂O) exhibited a repeating pattern in WW (Fig. 3 i + j, black symbols). After all three fertilization events, ap_N₂O ranged between 44 and 61 at% ¹⁵N decreasing continuously to 20–25 at% ¹⁵N until the next fertilization. In SB, ap_N₂O only reached 20 and 33 at% ¹⁵N after the first and second fertilization, respectively. Lowest ap_N₂O was 11.5 at% ¹⁵N measured on September 21st. After SB harvest and leaf incorporation, ap_N₂O values increased slightly reaching values of 22 at% ¹⁵N on October 18th, ¹⁵N enrichment of the total soil NO₃⁻ pool in the upper 20 cm (Fig. 3 i + j, red symbols) was mostly slightly lower than ap_N₂O.

The fraction of ¹⁵N-pool-derived N₂O (Fp_N₂O) showed a very similar pattern as the ¹⁵N-pool-derived N₂O fluxes and the denitrification product ratio for both crops (Fig. 3 g + h). Fp_N₂O increased from 0.15 in mid-June to 0.4 after WW harvest, then decreased to values close to 0. In SB, Fp_N₂O was >0.2 in the beginning of the measurement period, decreased towards 0 in July, and showed a peak of 0.4 parallel with the N₂O peak after incorporation of SB leaves.

Total N₂O and N₂O + N₂ production rates

Production-diffusion modeling was applied to calculate total production rates of N₂O, N₂, and N₂O + N₂ derived from the labeled ¹⁵N labeled pool. The correction factor for N fluxes ranged between 0.59 and 0.71 and was higher for smaller chambers and drier soils (Supplementary Figure S13). Modelled total production rates N₂O_prod, N₂_prod, and N₂O + N₂_prod followed very similar patterns than measured fluxes (Supplementary Figure S14).

Response of N₂O and N₂O + N₂ fluxes, and total N₂O ratios to soil variables

The applied generalized additive models (GAM, see Supplementary Tables: S3-S8) explained 57% of the variance in the log-scaled N₂O fluxes and 66% of the log-scaled N₂O + N₂_est fluxes in WW. For N₂O fluxes, we found a significant interaction between soil temperature and Nmin and a linear effect of WEOC. For the N₂O + N₂_est fluxes, the best model included soil moisture, temperature, and WEOC. Total N₂O ratios in WW depended on an interaction of soil moisture and temperature (pseudo-R² = 0.1997).

In the SB growing season without the post-harvest period, GAM explained 47% of the variance in the log-scaled N₂O fluxes and 79% of the log-scaled N₂O + N₂_est fluxes. For N₂O fluxes, soil temperature and Nmin were significant, while for the N₂O + N₂_est fluxes, an interaction between

soil moisture and temperature was found. Total N₂O ratios were positively correlated to N_{min} and WEOC and negatively correlated to soil temperature (pseudo-R² = 0.3152).

Cumulative N emissions and ¹⁵N recovery

Cumulative N₂O, N₂O + N₂, N₂O + N₂ _prod production, N₂O + N_est, and fertilizer-derived N₂O + N₂_fert emissions were higher in WW than in SB, although this was only significant for N₂O + N₂_est and fertilizer-derived N₂O + N₂_fert (Table 2). Fertilizer-derived N₂O + N₂_fert emissions accounted for 57.4 and 36.4% of ¹⁵N-pool-derived N₂O + N₂ emissions for WW and SB, respectively.

¹⁵N recovery in the plant biomass during the growing season is shown in Table 3. In WW, ¹⁵N recovery in the above-ground crop biomass was around 87%. In SB, ¹⁵N recovery in the plant biomass increased from 79 to > 90% during the growing season. When summing up the recovered ¹⁵N in the soil and plant pools, recovery rates were higher than 100% in both crops indicating that some pools were overestimated. In WW, the highest share of ¹⁵N was recovered in the wheat biomass (grains + straw), followed by the 0–30 cm soil layer. Similarly in SB, the highest share of ¹⁵N was recovered in the biomass (beets + leaves), followed by the 0–30 cm soil layer which included incorporated sugar beet leaves.

Discussion

Best estimates for N₂O + N₂ fluxes

N₂ concentration in the headspace atmosphere was mostly < 2% at sampling confirming that HeO₂ flushing of chambers worked very well and more effective than in the sandy soil employed by Well et al. (2019a). Using chambers to sample soil gas fluxes alters the diffusive flux from the soil to the surface and several approaches have been developed to correct from this bias during flux calculations (Parkin et al. 2012). Due to the long accumulation time that is needed to achieve ¹⁵N₂ concentrations above the detection limit and high cost of analysis, only one sample is taken to determine N₂ and N₂O + N₂ fluxes. However, with one time point for N₂O + N₂ fluxes, it is not possible to correct for non-linearity during flux calculations. In addition, we expect the diffusive loss to the subsoil to be more relevant for ¹⁵N-labelled gases as the formation of ¹⁵N-labelled denitrification products is limited to the soil volume amended with ¹⁵N-labelled NO₃⁻ (Well et al. 2019b). To overcome this, we applied production-diffusion modelling to calculate total N₂O and N₂ production within the soil column including subsoil fluxes.

Modelled N₂O + N₂_prod rates were about 3-times higher than measured surface N fluxes derived from the labeled ¹⁵N pool

Table 2 Cumulated N₂O and N₂O + N₂ losses of winter wheat (WW) and sugar beet (SB) plots. ‘N₂O + N₂ measured’ refers to measured values applying the ¹⁵NGF+, ‘N₂O + N₂ production’ refers to values calculated by applying production-diffusion modelling to measured values, and ‘N₂O + N₂_est’ refers to values calculated from total N₂O ratios and total N₂O fluxes. Means and standard error for n = 5. Different capital letters indicate statistically significant differences between crops (p ≤ 0.05)

Crop	N ₂ O (mg N m ⁻²)	N ₂ O + N ₂ measured (mg N m ⁻²)	N ₂ O + N ₂ production (mg N m ⁻²)	N ₂ O + N ₂ _est (mg N m ⁻²)	Ratio N ₂ O/ (N ₂ O + N ₂ _est)	Fertilizer-derived N ₂ O + N ₂ _fert (mg N m ⁻²)
WW	100.5 ± 27.3 A	538.5 ± 129.4 A	1651.5 ± 412.8 A	860.4 ± 220.9 B	0.118 ± 0.017 A	494.2 ± 119.3 B
SB	81.4 ± 19.0 A	440.4 ± 165.1 A	1290.4 ± 502.4 A	553.1 ± 96.3 A	0.146 ± 0.015 B	201.3 ± 3119 A

Table 3 Time course of recovered $^{15}\text{N}_{\text{excess}}$ in the mesoplots. Input refers to the ^{15}N input from fertilization and crop residues. Values in brackets indicate relative ^{15}N recovery in relation to ^{15}N input at that date. Means for $n=5$

	10.05.2021	09.08.2021	26.10.2021	
Winter Wheat				
Input ($\text{mg } ^{15}\text{N m}^{-2}$)	648.8	973.1	1112.2	
Straw ($\text{mg } ^{15}\text{N m}^{-2}$) [%]	561.8 [86.6]	446.6 [45.9]	8601.0 [77.4]	
Grain ($\text{mg } ^{15}\text{N m}^{-2}$) [%]		414.5 [42.6]		
Phacelia ($\text{mg } ^{15}\text{N m}^{-2}$) [%]			18.0 [1.6]	
Soil 0–30 ($\text{mg } ^{15}\text{N m}^{-2}$) [%]			260.9 [23.5]	
Soil 30–60 ($\text{mg } ^{15}\text{N m}^{-2}$) [%]			44.4 [4.0]	
Soil 60–90 ($\text{mg } ^{15}\text{N m}^{-2}$) [%]			13.1 [1.2]	
Sugar Beet	21.06.2021	24.08.2021	27.09.2021	26.10.2021
Input ($\text{mg } ^{15}\text{N m}^{-2}$)	231.7	463.4	463.4	628.3
Leaves ($\text{mg } ^{15}\text{N m}^{-2}$) [%]	128.7 [55.6]	248.0 [53.5]	221.7 [47.8]	395.9 [63.0]
Beet ($\text{mg } ^{15}\text{N m}^{-2}$) [%]	033.2 [14.3]	183.3 [39.6]	174.2 [7.6]	
Soil 0–30 ($\text{mg } ^{15}\text{N m}^{-2}$) [%]				187.1 [29.8]
Soil 30–60 ($\text{mg } ^{15}\text{N m}^{-2}$) [%]				11.5 [1.8]
Soil 60–90 ($\text{mg } ^{15}\text{N m}^{-2}$) [%]				5.3 [0.9]

showing to which extent the $^{15}\text{NGF}+$ could have underestimated total N losses in our field study. As this is the first plot-scale field study applying the $^{15}\text{NGF}+$ over a growing season, evaluation of our results in comparison to other studies is not possible. For the conventional ^{15}NGF , modelled subsurface flux was evaluated by comparing measurements with and without closing the ^{15}N labeled soil volume at the bottom to exclude subsoil fluxes (Well et al. 2019b). For the $^{15}\text{NGF}+$ this evaluation is still missing. To improve comparability of measured N_2 fluxes, further experiments comparing N_2O and N_2 production with and without HeO_2 flushing under broader conditions (soil texture, moisture, etc.) and including reference measurement with cylinders closed at the bottom are indispensable (Micucci et al. 2023).

In our study, denitrification product ratios of measured and corrected fluxes were very similar (Supplementary Figure S2), which is in agreement with Well et al. (2019a) reporting similar product ratios for classic ^{15}NGF and improved $^{15}\text{NGF}+$. Thus, our proposed conservative approach to estimate $\text{N}_2\text{O} + \text{N}_2$ losses based on total N_2O fluxes (see Eq. 4) and the total N_2O ratio gives the most reliable estimate of $\text{N}_2\text{O} + \text{N}_2$ losses for our study.

Effect of crop growth and development on soil parameters and N fluxes

Different temporal crop growth and development patterns strongly affected all controlling variables of denitrification in our field site. Especially during the early growth phase, SB soil moisture and temperature were higher than in WW, while during ripening and after harvest soil moisture was higher in WW. Soil temperature was a significant factor

explaining N_2O and $\text{N}_2\text{O} + \text{N}_2_{\text{est}}$ fluxes for both crops. Increasing soil temperatures accelerate the metabolism of microorganisms, promoting O_2 consumption by respiration and denitrification, especially when high soil moisture levels restrict O_2 availability (Betlach and Tiedje 1981; Senbayram et al. 2014). However, soil moisture was only a significant explanatory variable for $\text{N}_2\text{O} + \text{N}_2$ fluxes. High soil moisture decreases gas diffusion rates and thus restricts O_2 availability in soil leading to higher denitrification activities and higher N_2O reduction to N_2 (Davidson 1993; Scholefield et al. 1997; McKenney et al. 2001; Schlüter et al. 2018; Rohe et al. 2021), therefore affecting $\text{N}_2\text{O} + \text{N}_2_{\text{est}}$ fluxes. Product ratios in WW were in tendency higher during the summer months when soil temperatures and moisture were high as confirmed by the significant interaction between these driving factors.

High C_{org} availability in planted soils has been associated with high denitrification rates in several studies (Klemmedtsen et al. 1987; Philippot et al. 2009; Senbayram et al. 2020). Next to its role as electron donor during denitrification, increased C from rhizodeposition by growing plants stimulates microbial activity and respiration creating anaerobic zones in the rhizosphere favorable for denitrification (Firestone and Davidson 1989; Hamonts et al. 2013; Senbayram et al. 2020). While WW plants exude approximately 20–30% of assimilated C into the soil, SB plants store most translocated C in their beets (Kuzyakov and Domanski 2000; Ludwig et al. 2007). This was clearly visible in our study, where WEOC content in WW increased during the vegetative growth phase. After anthesis, decreased root exudation led to decreasing WEOC content with the onset of ripening

at the end of June. In contrast, SB plant growth did not affect WEOC content. Accordingly, we found that WEOC was a driving variable of N_2O and $N_2O + N_2$ fluxes in WW but not in SB.

Although available NO_3^- is known to be an important controlling factor for denitrification (von Rheinbaben and Trolldenier 1984; Haider et al. 1985; Groffman and Tiedje 1988; Luo et al. 1999; Rummel et al. 2021), soil mineral N (Nmin) only significantly affected N_2O fluxes, but not $N_2O + N_2$ fluxes in our field study. N uptake of cereals increases almost linearly between tillering and anthesis (Bashir et al. 1997; Lászitivity et al. 1984; Malhi et al. 2011), while N uptake of SB follows a sigmoid curve, with low N uptake in the first month after emergence (Cariolle and Duval 2006). Accordingly, Nmin content and N_2O fluxes remained low after first fertilization in WW, but strongly increased in SB. During the WW ripening phase, soil mineral N values increased, which is consistent with cereals reaching lowest N uptake rates during ripening (Bashir et al. 1997; Lászitivity et al. 1984; Malhi et al. 2011). Higher Nmin content and increasing soil temperatures promoted N_2O and $N_2O + N_2$ fluxes during summer months in WW. In contrast, Nmin did not increase after the second fertilization in SB. Maximum N uptake rates of SB are $0.35 - 0.55 \text{ g N m}^{-2} \text{ d}^{-1}$ (Hoffmann et al. 2021) and caused nearly complete uptake of the fertilized 5 g N m^{-2} within the six days from fertilization to the next soil sampling limiting Nmin availability and restricting N_2O formation in SB in the summer months. Post-harvest N_2O and $N_2O + N_2$ losses were high in both crops as dead roots and plant residues promote local oxygen shortage due to increased microbial respiration and higher Corg supply (Parkin 1987; Chen et al. 2013; Kravchenko et al. 2018).

Overall, N fluxes were highest when SB plants were small, during ripening of WW, and after harvest of both crops, i.e. in phases of low/slow plant N and water uptake, and higher soil temperatures. While climatic and meteorological conditions strongly control boundary conditions for denitrification in general, crop growth and development are crucial controlling factors that need to be implemented in modelling to better understand and predict dynamics of N_2O and N_2 fluxes on the field scale.

Pools and processes contributing to N losses

Different N pools and N turnover processes contributed to N_2O formation throughout the experiment in both crops. After WW fertilization, the ^{15}N enrichment of the total soil NO_3^- pool in the 0–20 cm soil layer ($^{15}a_NO_3^-$) in the microplots was in the range of the targeted value of 50–60 at% which was also reflected in ap_N_2O around 60 at% confirming homogenous labeling of the upper 20 cm soil layer. After fertilization, $^{15}a_NO_3^-$ decreased, as unlabeled

organic N was mineralized and diluted the labeled NO_3^- pool (Buchen et al. 2016; Deppe et al. 2017; Rummel et al. 2021). Simultaneously, ap_N_2O decreased indicating that also the ^{15}N -labeled NO_3^- pool undergoing denitrification was diluted by mineralized unlabeled NO_3^- . This was even more pronounced in the SB field site, where due to the high initial soil mineral N content and strong ongoing mineralization, $^{15}a_NO_3^-$ in the microplots only reached 20 at% after fertilization and then rapidly decreased to 10 at% after fertilization. Accordingly, denitrification of unlabeled NO_3^- , as well as nitrification, nitrifier denitrification, and coupled nitrification–denitrification may have contributed to N_2O formation in both crops (Wrage et al. 2001; van Groenigen et al. 2015; Wrage-Mönnig et al. 2018). Overall, ap_N_2O was in tendency higher than $^{15}a_NO_3^-$ in the microplots indicating that N_2O was mostly emitted from hotspots with a ^{15}N enrichment higher than the average soil NO_3^- pool. This indicates that N_2O was predominately lost from microsites that were more anoxic and thus less diluted with nitrification-derived unlabeled NO_3^- (Deppe et al. 2017; Rummel et al. 2021). Further, we can exclude fungal co-denitrification as a possible source, as this would lead to ap_N_2O lower than $^{15}a_NO_3^-$ due to hybrid formation of N_2O or N_2 (Spott and Stange 2007).

A low fraction of N_2O lost from the ^{15}N -labelled NO_3^- pool undergoing denitrification ($Fp_N_2O < 0.4$) further indicated strong contribution of non-labeled pools to N_2O formation throughout the experiment. Fp_N_2O increased in WW during the summer months. High soil and air temperatures and slow/low plant N and water uptake during ripening and after harvest increased total and ^{15}N -pool-derived N_2O fluxes leading to higher denitrification product ratios and Fp_N_2O .

In contrast, in SB, Fp_N_2O was especially low during the summer months, when N_2O and $N_2O + N_2$ fluxes were low. Rapid plant N uptake limited soil N availability and low soil moisture ~40% WFPS further restricted denitrification. Measured N_2O fluxes during this time likely derived partly from nitrification (Davidson 1993; Stremińska et al. 2012). Incorporation of ^{15}N labeled SB leaves slightly increased ap_N_2O , and strongly increased Fp_N_2O and total N_2O ratio indicating that the increase in N_2O derived from the ^{15}N labeled N pool including the added SB leaves. This confirms that plant litter is an important driver of denitrification contributing to N_2O and N_2 losses through both increased N availability and increased O_2 consumption (Parkin 1987; Chen et al. 2013; Kravchenko et al. 2018).

Cumulative N losses and balance – differences between crops

WW and SB differed in their growing patterns which was reflected in the time course of N_2O and $N_2O + N_2$ production and emissions. Cumulative N_2O emissions and average

daily N_2O losses were similar for WW and SB. This can largely be related to high N losses during early SB growth and after harvest. High N availability after incorporation of the catch crop would have made fertilization after sowing obsolete. This was further confirmed by a low share of fertilizer-derived $N_2O + N_2$ losses in SB. However, we needed to add labeled $^{15}NO_3^-$ fertilizer to allow determination of N_2 fluxes with the ^{15}N gas flux method. Further, N fertilization before or shortly after SB sowing is common management practice in Germany and was applied on the SB field site surrounding this experiment.

In both crops, the highest share of ^{15}N was recovered in plant biomass. ^{15}N recovery at the end of the experiment was above 100% for WW indicating overestimation of N recovery in some of the pools. In WW, it was difficult to clearly define the subplot for harvest due to large and uneven plant growth. Highest recovery in soil was in the 0–30 cm layer, including residual fertilizer in WW and SB leaves in SB. In WW, some ^{15}N was also recovered in deeper soil layers including 60–90 pointing towards leaching of fertilized N due to low plant uptake rates after the second and third fertilization. Estimating soil ^{15}N content was difficult due to large heterogeneity, especially after SB leaf incorporation and may have contributed to uncertainty in total ^{15}N recovery. Data quality of ^{15}N budgets did not allow comparison of N_2 losses and unrecovered N in the N balance in our field trial but should be included in future studies.

Conclusions

This is the first plot-scale field study over a growing season confirming that the improved ^{15}N gasflux method with HeO_2 flushing and production-diffusion modeling presents a promising tool to monitor N_2 production and losses on the field scale. Future studies should include comparisons with and without HeO_2 flushing under broader conditions (soil texture, crop species) and include reference measurements with cylinders closed at the bottom. Growing plants affected all controlling factors of denitrification, and dynamics clearly differed between crop species. Overall, N_2O and N_2 emissions were highest when plant N and water uptake were low, i.e., during early growth stages, ripening, and after harvest indicating that crop growth and development could be used to predict probability of $N_2O + N_2$ losses in biogeochemical models.

Supplementary Information The online version contains supplementary material available at <https://doi.org/10.1007/s00374-024-01806-z>.

Acknowledgements This study would not have been possible without the help and support of many people. We want to thank (Turbo-) Thade Potthoff for help with field work and sampling, the team of the experimental station Reinshof, especially Jonas Kirschner and Philip Kempf,

for managing the field site, Ulrike Kierbaum for mineral N analysis, Karin Schmidt for WEOC analysis, Caroline Buchen-Tschiskale and Martina Heuer for IRMS analysis of gas samples, Jens Dyckmans, Lars Szewc, and Reinhard Langel for IRMS analysis of plant, soil, and mineral N samples, Daniel Ziehe and Kerstin Gilke for GC analysis of gas samples, Rosanna Schneider, Johannes Cordes, Simone Urstadt, and Susanne Koch for help with sample preparation and laboratory work, Reinhard Hilmer for support on field work, and Hildegard for reliable power supply. We want to thank two anonymous reviewers for their very detailed and constructive feedback on the manuscript.

Author contributions Conceptualization: PSR, KD; Methodology: RW, AM, PSR; Investigation: JE, PSR; Data analysis (soil, plant, gas fluxes): JE, PSR; Data analysis (^{15}NGF): RW; Diffusion-production modelling: MM; Writing—original draft preparation: JE, PSR; Writing—review and editing: PSR, RW, AM; Funding acquisition: KD, RW; Supervision: PSR, AM; all authors have read and agreed to the published version of the manuscript.

Funding Open Access funding enabled and organized by Projekt DEAL. This research work was supported by the Deutsche Forschungsgemeinschaft through the research unit DFG-FOR 2337: Denitrification in Agricultural Soils: Integrated Control and Modelling at Various Scales (DASIM, grant numbers DI 546/4–2, We 1904/10–2). Open Access funding enabled and organized by Projekt DEAL.

Data availability The datasets generated during the current study are available at <https://doi.org/https://doi.org/10.25625/ZFUXGR>. Please contact the corresponding author for further details.

Declarations

Competing Interests The authors have no conflicts of interest to declare that are relevant to the content of this article.

Open Access This article is licensed under a Creative Commons Attribution 4.0 International License, which permits use, sharing, adaptation, distribution and reproduction in any medium or format, as long as you give appropriate credit to the original author(s) and the source, provide a link to the Creative Commons licence, and indicate if changes were made. The images or other third party material in this article are included in the article's Creative Commons licence, unless indicated otherwise in a credit line to the material. If material is not included in the article's Creative Commons licence and your intended use is not permitted by statutory regulation or exceeds the permitted use, you will need to obtain permission directly from the copyright holder. To view a copy of this licence, visit <http://creativecommons.org/licenses/by/4.0/>.

References

- Bashir R, Norman RJ, Bacon RK, Wells BR (1997) Accumulation and Redistribution of Fertilizer Nitrogen-15 in Soft Red Winter Wheat. *Soil Sci Soc Am J* 61:1407–1412. <https://doi.org/10.2136/sssaj1997.03615995006100050018x>
- Bergsma TT, Ostrom NE, Emmons M, Robertson GP (2001) Measuring Simultaneous Fluxes from Soil of N_2O and N_2 in the Field Using the 15 N-Gas “Nonequilibrium” Technique. *Environ Sci Technol* 35:4307–4312. <https://doi.org/10.1021/es010885u>
- Betlach MR, Tiedje JM (1981) Kinetic Explanation for Accumulation of Nitrite, Nitric Oxide, and Nitrous Oxide During Bacterial Denitrification. *Appl Environ Microbiol* 42:1074–1084. <https://doi.org/10.1128/aem.42.6.1074-1084.1981>

- Buchen C, Lewicka-Szczepak D, Fuß R, Helfrich M, Flessa H, Well R (2016) Fluxes of N₂ and N₂O and contributing processes in summer after grassland renewal and grassland conversion to maize cropping on a Plaggic Anthrosol and a Histic Gleysol. *Soil Biol Biochem* 101:6–19. <https://doi.org/10.1016/j.soilbio.2016.06.028>
- Buchen-Tschiskale C, Well R, Flessa H (2023) Tracing nitrogen transformations during spring development of winter wheat induced by 15N labeled cattle slurry applied with different techniques. *Sci Total Environ* 871:162061. <https://doi.org/10.1016/j.scitotenv.2023.162061>
- Cariolle M, Duval R (2006) Nutrition - Nitrogen. In: Draycott AP (ed) *Sugar Beet*. Blackwell Publishing Ltd, Oxford, pp 169–184
- Chen H, Li X, Hu F, Shi W (2013) Soil nitrous oxide emissions following crop residue addition: a meta-analysis. *Glob Chang Biol* 19:2956–2964. <https://doi.org/10.1111/gcb.12274>
- Ciais P, Sabine C, Bala G (2014) Carbon and other biogeochemical cycles. *Glob Clim Chang* 2014:465–469. <https://doi.org/10.1017/CBO9781107415324.015>
- Cribari-Neto F, Zeileis A (2010) Beta Regression in R. *J Stat Softw* 34:1–24. <https://doi.org/10.18637/jss.v034.i02>
- Davidson EA (1993) Soil Water Content and the Ratio of Nitrous Oxide to Nitric Oxide Emitted from Soil. *Biogeochem Glob Chang* 369–386. https://doi.org/10.1007/978-1-4615-2812-8_20
- Deppe M, Well R, Giesemann A, Spott O, Flessa H (2017) Soil N₂O fluxes and related processes in laboratory incubations simulating ammonium fertilizer depots. *Soil Biol Biochem* 104:68–80. <https://doi.org/10.1016/j.soilbio.2016.10.005>
- DWD Deutscher Wetterdienst (2021). https://opendata.dwd.de/climate_environment/CDC/observations_germany; last accessed 04.01.2022
- Dyckmans J, Eschenbach W, Langel R, Szwec L, Well R (2021) Nitrogen isotope analysis of aqueous ammonium and nitrate by membrane inlet isotope ratio mass spectrometry (MIRMS) at natural abundance levels. *Rapid Commun Mass Spectrom*. <https://doi.org/10.1002/rcm.9077>
- Eschenbach W, Lewicka-Szczepak D, Stange CF, Dyckmans J, Well R (2017) Measuring 15 N Abundance and Concentration of Aqueous Nitrate, Nitrite, and Ammonium by Membrane Inlet Quadrupole Mass Spectrometry. *Anal Chem* 89:6076–6081. <https://doi.org/10.1021/acs.analchem.7b00724>
- Eschenbach W, Well R, Dyckmans J (2018) NO Reduction to N₂O Improves Nitrate 15 N Abundance Analysis by Membrane Inlet Quadrupole Mass Spectrometry. *Anal Chem* 90:11216–11218. <https://doi.org/10.1021/acs.analchem.8b02956>
- Firestone MK, Davidson EA (1989) Microbiological basis of NO and N₂O production and consumption in soil. In: Andreae MO, Schimel DS (eds) *Report of the Dahlem Workshop on Exchange of Trace Gases between Terrestrial Ecosystems and the Atmosphere*. John Wiley and Sons, Chichester, pp 7–21
- Folorunso OA, Rolston DE (1984) Spatial Variability of Field-Measured Denitrification Gas Fluxes. *Soil Sci Soc Am J* 48:1214–1219. <https://doi.org/10.2136/sssaj1984.03615995004800060002x>
- Friedl J, Cardenas LM, Clough TJ, Dannenmann M, Chunsheng H, Scheer C (2020) Measuring denitrification and the N₂O:(N₂O + N₂) emission ratio from terrestrial soils. *Curr Opin Environ Sustain* 47:61–71. <https://doi.org/10.1016/j.cosust.2020.08.006>
- Friedl J, Deltedesco E, Keiblinger KM, Gorfer M, De Rosa D, Scheer C, Grace PR, Rowlings DW (2022) Amplitude and frequency of wetting and drying cycles drive N₂ and N₂O emissions from a subtropical pasture. *Biol Fertil Soils* 58:593–605. <https://doi.org/10.1007/s00374-022-01646-9>
- Friedl J, Warner D, Wang W, Rowlings DW, Grace PR, Scheer C (2023) Strategies for mitigating N₂O and N₂ emissions from an intensive sugarcane cropping system. *Nutr Cycl Agroecosystems* 125:295–308. <https://doi.org/10.1007/s10705-023-10262-4>
- Fuß R (2020) gasfluxes: Greenhouse Gas Flux Calculation from Chamber Measurements
- Groffman PM, Tiedje JM (1988) Denitrification Hysteresis During Wetting and Drying Cycles in Soil. *Soil Sci Soc Am J* 52:1626–1629. <https://doi.org/10.2136/sssaj1988.03615995005200060022x>
- Groffman PM, Tiedje JM, Robertson GP, Christensen S (1988) Denitrification at different temporal and geographical scales: Proximal and distal controls. In: Wilson JR (ed) *Advances in Nitrogen Cycling in Agricultural Ecosystems*. CAB International, Wallingford, pp 174–192
- Grosz B, Well R, Dechow R, Köster JR, Khalil MI, Merl S, Rode A, Ziehmer B, Matson A, Hongxing H (2021) Evaluation of denitrification and decomposition from three biogeochemical models using laboratory measurements of N₂, N₂O and CO₂. *Biogeosciences* 18:5681–5697. <https://doi.org/10.5194/bg-18-5681-2021>
- Grosz BP, Matson A, Butterbach-Bahl K, Clough T, Davidson EA, Dechow R, DelGrosso A, Diamantopoulos E, Dörsch P, Haas E, He H, Henri VD, Hui D, Kleinedam K, Kraus D, Duhnert M, Léonard J, Müller C, Petersen SO, Sihi D, Vogeler I, Well R, Yeluripati J, Zhang J, Scheer C (2023) Modeling denitrification: can we report what we don't know? *AGU Adv – ESS Open Arch*. <https://doi.org/10.1029/2023AV000990>
- Haider K, Mosier A, Heinemeyer O (1985) Phytotron Experiments to Evaluate the Effect of Growing Plants on Denitrification. *Soil Sci Soc Am J* 49:636–641
- Hamonts K, Clough TJ, Stewart A, Clinton PW, Richardson AL, Wakelin SA, O'Callaghan M, Condon LM (2013) Effect of nitrogen and waterlogging on denitrifier gene abundance, community structure and activity in the rhizosphere of wheat. *FEMS Microbiol Ecol* 83:568–584. <https://doi.org/10.1111/1574-6941.12015>
- Hoffmann C, Koch H-J, Märkländer B (2021) Sugar beet. In: Sadras VO, Calderini DF (eds) *Crop Physiology - Case Histories for Major Crops*. Academic Press
- Hutchinson G, Mosier A (1981) Improved soil cover method for field measurement of nitrous oxide fluxes. *Soil Sci Soc Am J* 45:311–316
- Jeuffroy MH, Baranger E, Carrouée B, de Chezelles E, Gosme M, Hénault C, Schneider A, Cellier P (2013) Nitrous oxide emissions from crop rotations including wheat, oilseed rape and dry peas. *Biogeosciences* 10:1787–1797. <https://doi.org/10.5194/bg-10-1787-2013>
- Katz I, Caillibotte G, Martin AR, Arpentiner P (2011) Property value estimation for inhaled therapeutic binary gas mixtures: He, Xe, N₂O, and N₂ with O₂. *Med Gas Res* 1:1–12. <https://doi.org/10.1186/2045-9912-1-28/TABLES/11>
- Kirkby R, Friedl J, Takeda N, De Rosa D, Rowlings DW, Grace PR (2023) Nonlinear response of N₂O and N₂ emissions to increasing soil nitrate availability in a tropical sugarcane soil. *J Soils Sediments* 2065–2071. <https://doi.org/10.1007/s11368-023-03482-2>
- Klemedtsson L, Svensson BH, Rosswall T (1987) Dinitrogen and nitrous oxide produced by denitrification and nitrification in soil with and without barley plants. *Plant Soil* 99:303–319. <https://doi.org/10.1007/BF02370877>
- Kravchenko AN, Fry JE, Guber AK (2018) Water absorption capacity of soil-incorporated plant leaves can affect N₂O emissions and soil inorganic N concentrations. *Soil Biol Biochem* 121:113–119. <https://doi.org/10.1016/j.soilbio.2018.03.013>
- Kuzyakov Y, Domanski G (2000) Carbon input by plants into the soil. *Review J Plant Nutr Soil Sci* 163:421–431. [https://doi.org/10.1002/1522-2624\(200008\)163:4%3c421::AID-JPLN421%3e3.0.CO;2-R](https://doi.org/10.1002/1522-2624(200008)163:4%3c421::AID-JPLN421%3e3.0.CO;2-R)
- Lancashire PD, Bleiholder H, van den Boom T, Langelüddeke P, Stauss R, Weber E, Witzemberger A (1991) A uniform decimal code for growth stages of crops and weeds. *Ann Appl Biol* 119:561–601. <https://doi.org/10.1111/j.1744-7348.1991.tb04895.x>

- László B, Biczók G, Ruda M (1984) Evaluation of Dry Matter and Nutrient Accumulation in Winter Wheat. *Cereal Res Commun* 12:193–199
- Lewicka-Szczepak D, Well R, Giesemann A, Rohe L, Wolf U (2013) An enhanced technique for automated determination of ^{15}N signatures of N_2 , $(\text{N}_2+\text{N}_2\text{O})$ and N_2O in gas samples. *Rapid Commun Mass Spectrom* 27:1548–1558. <https://doi.org/10.1002/rcm.6605>
- Lewicka-Szczepak D, Well R, Köster JR, Fuß R, Senbayram M, Dittert K, Flessa H (2014) Experimental determinations of isotopic fractionation factors associated with N_2O production and reduction during denitrification in soils. *Geochim Cosmochim Acta* 134:55–73. <https://doi.org/10.1016/j.gca.2014.03.010>
- Ludwig B, Schulz E, Rethemeyer J, Merbach I, Flessa H (2007) Predictive modelling of C dynamics in the long-term fertilization experiment at Bad Lauchstädt with the Rothamsted Carbon Model. *Eur J Soil Sci* 58:1155–1163. <https://doi.org/10.1111/j.1365-2389.2007.00907.x>
- Luo J, Tillman RW, Ball PR (1999) Factors regulating denitrification in a soil under pasture. *Soil Biol Biochem* 31:913–927. [https://doi.org/10.1016/S0038-0717\(99\)00013-9](https://doi.org/10.1016/S0038-0717(99)00013-9)
- Malhi SS, Johnston AM, Schoenau JJ, Wang ZH, Vera CL (2011) Seasonal biomass accumulation and nutrient uptake of wheat, barley and oat on a Black Chernozem Soil in Saskatchewan. *Can J Plant Sci* 86:1005–1014. <https://doi.org/10.4141/p05-116>
- Malique F, Ke P, Böttcher J, Dannenmann M, Butterbach-Bahl K (2019) Interactive plant and soil effects on denitrification potential in agricultural soils. *Plant Soil* 20:6603
- McKenney DJ, Drury CF, Wang SW (2001) Effects of Oxygen on Denitrification Inhibition, Repression, and Derepression in Soil Columns. *Soil Sci Soc Am J* 65:126–132. <https://doi.org/10.2136/sssaj2001.651126x>
- Micucci G, Sgouridis F, McNamara NP, Krause S, Lynch I, Roos F, Well R, Ullah S (2023) The ^{15}N -Gas flux method for quantifying denitrification in soil: Current progress and future directions. *Soil Biol Biochem* 109108. <https://doi.org/10.1016/j.soilbio.2023.109108>
- Mulvaney RL (1984) Determination of ^{15}N -Labeled Dinitrogen and Nitrous Oxide With Triple-Collector Mass Spectrometers. *Soil Sci Soc Am J* 48:690–692. <https://doi.org/10.2136/sssaj1984.03615995004800030045x>
- Parkin TB (1987) Soil Microsites as a Source of Denitrification Variability. *Soil Sci Soc Am J* 51:1194–1199. <https://doi.org/10.2136/sssaj1987.03615995005100050019x>
- Parkin TB, Venterea RT, Hargreaves SK (2012) Calculating the Detection Limits of Chamber-based Soil Greenhouse Gas Flux Measurements. *J Environ Qual* 41:705–715. <https://doi.org/10.2134/jeq2011.0394>
- Patrignani A, Ochsner TE (2015) Canopeo: A powerful new tool for measuring fractional green canopy cover. *Agron J* 107:2312–2320. <https://doi.org/10.2134/agronj15.0150>
- Philippot L, Hallin S, Börjesson G, Baggs EM (2009) Biochemical cycling in the rhizosphere having an impact on global change. *Plant Soil* 321:61–81. <https://doi.org/10.1007/s11104-008-9796-9>
- R Core Team (2022) R: A Language and Environment for Statistical Computing
- Rohe L, Apelt B, Vogel H-J, Well R, Wu G-M, Schlüter S (2021) Denitrification in soil as a function of oxygen supply and demand at the microscale. *Biogeosciences* 1–32. <https://doi.org/10.5194/bg-18-1185-2021>
- Rummel PS, Well R, Pfeiffer B, Dittert K, Floßmann S, Pausch J (2021) Nitrate uptake and carbon exudation – do plant roots stimulate or inhibit denitrification? *Plant Soil* 459:217–233. <https://doi.org/10.1007/s11104-020-04750-7>
- Ruser R, Fuß R, Andres M, Hegewald H, Kesenheimer K, Köbke S, Rübiger T, Quinones TS, Augustin J, Christen O, Dittert K, Kage H, Lewandowski I, Prochnow A, Stichnothe H, Flessa H (2017) Nitrous oxide emissions from winter oilseed rape cultivation. *Agric Ecosyst Environ* 249:57–69. <https://doi.org/10.1016/j.agee.2017.07.039>
- Scheer C, Fuchs K, Pelster DE, Butterbach-Bahl K (2020) Estimating global terrestrial denitrification from measured $\text{N}_2\text{O}:(\text{N}_2\text{O} + \text{N}_2)$ product ratios. *Curr Opin Environ Sustain* 47:72–80. <https://doi.org/10.1016/J.COSUST.2020.07.005>
- Schlüter S, Henjes S, Zawallich J, Bergaust L, Horn M, Ippisch O, Vogel H-J, Dörsch P (2018) Denitrification in Soil Aggregate Analogues—Effect of Aggregate Size and Oxygen Diffusion. *Front Environ Sci* 6:1–10. <https://doi.org/10.3389/fenvs.2018.00017>
- Scholefield D, Hawkins JMBB, Jackson SM (1997) Development of a helium atmosphere soil incubation technique for direct measurement of nitrous oxide and dinitrogen fluxes during denitrification. *Soil Biol Biochem* 29:1345–1352. [https://doi.org/10.1016/S0038-0717\(97\)00021-7](https://doi.org/10.1016/S0038-0717(97)00021-7)
- Senbayram M, Chen R, Wienforth B, Herrmann A, Kage H, Mühlhag KH, Dittert K (2014) Emission of N_2O from Biogas Crop Production Systems in Northern Germany. *Bioenergy Res* 7:1223–1236. <https://doi.org/10.1007/s12155-014-9456-2>
- Senbayram M, Well R, Shan J, Bol R, Burkhart S, Jones DL, Wu D (2020) Rhizosphere processes in nitrate-rich barley soil tripled both N_2O and N_2 losses due to enhanced bacterial and fungal denitrification. *Plant Soil* 448:509–522. <https://doi.org/10.1007/s11104-020-04457-9>
- Sgouridis F, Stott A, Ullah S (2016) Application of the ^{15}N gas-flux method for measuring in situ N_2 and N_2O fluxes due to denitrification in natural and semi-natural terrestrial ecosystems and comparison with the acetylene inhibition technique. *Biogeosciences* 13:1821–1835. <https://doi.org/10.5194/bg-13-1821-2016>
- Siegel RS, Hauck RD, Kurtz LT (1982) Determination of $^{30}\text{N}_2$ and Application to Measurement of N_2 Evolution During Denitrification. *Soil Sci Soc Am J* 46:68. <https://doi.org/10.2136/sssaj1982.03615995004600010013x>
- Spott O, Stange CF (2007) A new mathematical approach for calculation the contribution of anammox, denitrification and atmosphere to an N_2 mixture based on a ^{15}N tracer technique. *Rapid Commun Mass Spectrom* 21:2398–2406. <https://doi.org/10.1002/rcm>
- Spott O, Russow R, Apelt B, Stange CF (2006) A ^{15}N -aided artificial atmosphere gas flow technique for online determination of soil N_2 release using the zeolite Köstrolith SX6. *Rapid Commun Mass Spectrom* 20:3267–3274. <https://doi.org/10.1002/rcm>
- Stremińska MA, Felgate H, Rowley G, Richardson DJ, Baggs EM (2012) Nitrous oxide production in soil isolates of nitrate-ammonifying bacteria. *Environ Microbiol Rep* 4:66–71. <https://doi.org/10.1111/j.1758-2229.2011.00302.x>
- Takeda N, Friedl J, Kirkby R, Rowlings D, De Rosa D, Scheer C, Grace P (2022) Interaction between soil and fertiliser nitrogen drives plant nitrogen uptake and nitrous oxide (N_2O) emissions in tropical sugarcane systems. *Plant Soil* 477:647–663. <https://doi.org/10.1007/s11104-022-05458-6>
- Takeda N, Friedl J, Kirkby R, Rowlings D, Scheer C, De Rosa D, Grace P (2023) Denitrification Losses in Response to N Fertilizer Rates—Integrating High Temporal Resolution N_2O , In Situ $^{15}\text{N}_2\text{O}$ and $^{15}\text{N}_2$ Measurements and Fertilizer ^{15}N Recoveries in Intensive Sugarcane Systems. *J Geophys Res Biogeosciences* 128:1–15. <https://doi.org/10.1029/2023JG007391>
- van Groenigen JW, Huygens D, Boeckx P, Kuyper ThW, Lubbers IM, Rütting T, Groffman PM (2015) The soil N cycle: New insights and key challenges. *Soil* 1:235–256. <https://doi.org/10.5194/soil-1-235-2015>

- von Rheinbaben W, Trolldenier G (1984) Influence of plant growth on denitrification in relation to soil moisture and potassium nutrition. *Zeitschrift Für Pflanzenernährung Und Bodenkd* 147:730–738. <https://doi.org/10.1002/jpln.19841470610>
- Well R, Burkart S, Gieseemann A, Grosz BP, Köster JR, Lewicka-Szczebak D (2019a) Improvement of the ^{15}N gas flux method for in situ measurement of soil denitrification and its product stoichiometry. *Rapid Commun Mass Spectrom* 33:437–448. <https://doi.org/10.1002/rcm.8363>
- Well R, Maier M, Lewicka-Szczebak D, Köster JR, Ruoss N (2019b) Underestimation of denitrification rates from field application of the ^{15}N gas flux method and its correction by gas diffusion modelling. *Biogeosciences* 16:2233–2246. <https://doi.org/10.5194/bg-16-2233-2019>
- Wood SN, Augustin NH (2002) GAMs with integrated model selection using penalized regression splines and applications to environmental modelling. *Ecol Modell* 157:157–177. [https://doi.org/10.1016/S0304-3800\(02\)00193-X](https://doi.org/10.1016/S0304-3800(02)00193-X)
- Wood SN (2011) Fast stable restricted maximum likelihood and marginal likelihood estimation of semiparametric generalized linear models. *J R Stat Soc Ser B (Statistical Methodol)* 73:3–36. <https://doi.org/10.1111/j.1467-9868.2010.00749.x>
- Wrage N, Velthof GL, van Beusichem ML, Oenema O (2001) The role of nitrifier denitrification in the production of nitrous oxide. *Soil Biol Biochem* 33:1723–1732. [https://doi.org/10.1016/S0038-0717\(01\)00096-7](https://doi.org/10.1016/S0038-0717(01)00096-7)
- Wrage-Mönnig N, Horn MA, Well R, Müller C, Velthoff GL, Oenema O (2018) The role of nitrifier denitrification in the production of nitrous oxide revisited. *Soil Biol Biochem* 123:A3–A16. <https://doi.org/10.1016/j.soilbio.2018.03.020>

Publisher's Note Springer Nature remains neutral with regard to jurisdictional claims in published maps and institutional affiliations.